ACS Sustainable Chemistry & Engineering

Research Article

Cite This: ACS Sustainable Chem. Eng. 2018, 6, 9866−9875

Superhydrophobic Shish-kebab Membrane with Self-Cleaning and Oil/Water Separation Properties

Shuangjie Sun,[†] Liya Zhu,[†] Xianhu Liu,[*,‡] Lili Wu,[§] Kun Dai,[†] Chuntai Liu,[‡] Changyu Shen,[‡] Xingkui Guo,[§,⊥] Guoqiang Zheng,[*,†] and Zhanhu Guo[*,§]

[†]College of Materials Science and Engineering, The Key Laboratory of Material Processing and Mold of Ministry of Education, Zhengzhou University, No. 97 Wenhua Rd, Zhengzhou 450001, PR China

[‡]National Engineering Research Center for Advanced Polymer Processing Technology, The Key Laboratory of Advanced Materials Processing & Mold of Ministry of Education, Zhengzhou University, No. 100 Kexue Rd, Zhengzhou 450001, PR China

[§]Integrated Composites Laboratory (ICL), Department of Chemical & Biomolecular Engineering, University of Tennessee, 1015 Volunteer Boulevard, Knoxville, Tennessee 37996, United States

[⊥]College of Chemical and Environmental Engineering, Shandong University of Science and Technology, 579 Qianwangang Road, Qingdao 266590, China

Supporting Information

ABSTRACT: In nature, the water-repellent surface of a superhydrophobic material such as lotus has the micro/nano hierarchical structure, while shish-kebab, which is one of the most fascinating superstructure crystals in polymer science, also exhibits micro/nano hierarchical structure. Accordingly, it remains an idea of whether this structure can be used as the superhydrophobic materials. In this work, a modified flow-induced crystallization method was employed to fabricate a pure shish-kebab membrane, whose wetting behavior and other related performances were comprehensively studied. The membrane surface displays superhydrophobic characteristic with a static water contact angle of 161° and sliding angle of 3°. More importantly, the superhydrophobic membrane not only is of low adhesive, anti-impact, and self-cleaning performance, but also presents oil/water separation capacity, high absorption capacity with porosity (67−83%), and recyclability for organic liquids. This work proposed a new approach from the viewpoint of shish-kebab aggregation to construct a micro/nano structure in the polymer membrane with superhydrophobicity and other functional properties.

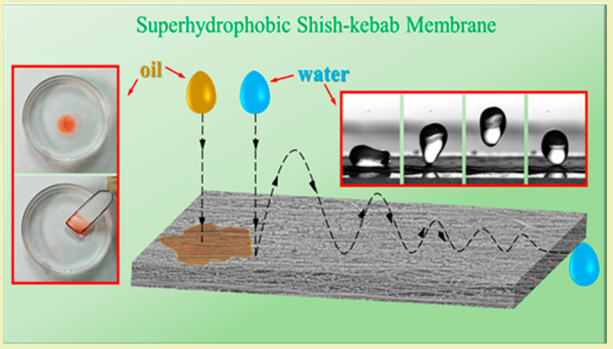

KEYWORDS: *Shish-kebab, Superhydrophobic, Self-cleaning, Oil/water separation*

INTRODUCTION

The superhydrophobic surface, on which the water droplet can form a contact angle larger than 150° and sliding angle lower than 10°, has aroused intensive interests, mainly inspired by the nature of a water-repellent surface.[1−5] Such a superhydrophobic surface generally shows performances of biomimicking antisticking, contamination prevention, water repellency, self-cleaning, and oil/water separation.[3,6−8] The methods to achieve a superhydrophobic surface include two steps, namely, the construction of rough structures and chemical modification with low-surface-energy materials.[9−13] Recently, some artificial techniques have been successfully employed to prepare superhydrophobic surfaces, including chemical etching,[14−16] colloidal coating,[17,18] anodic oxidation,[19] layer-by-layer deposition,[20] polymer reconformation,[21−23] electrospinning,[24] and templating.[25,26] However, the existing drawbacks (e.g., high-cost, low-efficiency, tedious, and time-consuming treatments, or processing with intricate instruments) have obstructed their further practical applications.[27]

As well-known, ultrahigh molecular weight polyethylene (UHMWPE) is a kind of high-performance polymer, showing high strength, high tensile modulus, and low density, which has attracted considerable interests.[28,29] Nowadays, UHMWPE is successfully used in some fields because of its unique properties, such as biocompatibility, chemical resistance, and electric insulation.[30] However, one of the main issues is that UHMWPE cannot be processed by conventional melt processing methods (e.g., injection molding, extrusion, and so on) because of its extremely high viscosity.[30] Therefore, UHMWPE is always processed by a solution processing method. In the past few years, many researchers have focused

Received: March 7, 2018
Revised: June 14, 2018
Published: June 15, 2018

DOI: 10.1021/acssuschemeng.8b01047
ACS Sustainable Chem. Eng. 2018, 6, 9866−9875

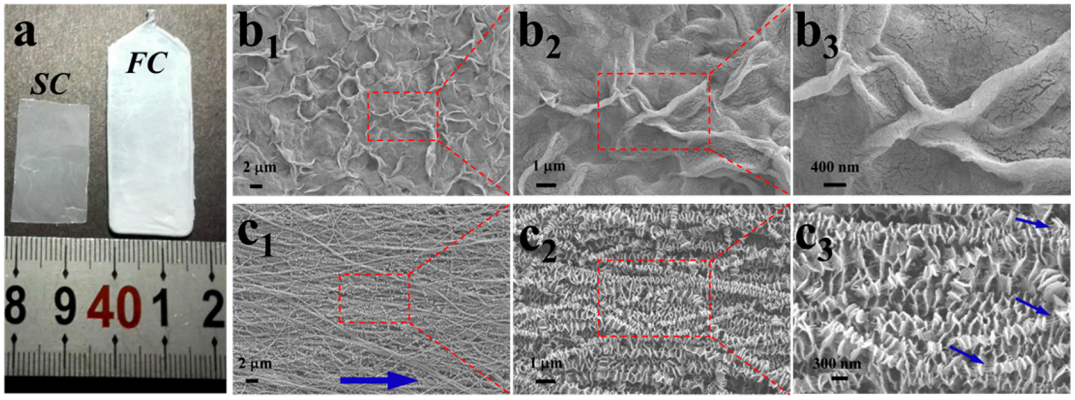

Figure 1. Surface morphology of SC and FC. (a) Digital photograph of SC and FC. Low- and high-magnified SEM images of (b_1–b_3) SC and (c_1–c_3) FC surfaces, the blue arrows refer to the flow direction in (c_1).

on fabricating superhydrophobic polymeric surfaces, governed by both the chemical composition and micro/nano hierarchical structure of the surface.[21−26] It is well-known that flow-induced crystallization is another effective method to build superstructures of polymer crystals.[31−34] For instance, shish-kebab, one of the most fascinating superstructures of polymer crystals, is composed of threadlike cores encircled with disc-like lamellar crystals.[34−36] However, it is difficult to fabricate a pure shish-kebab aggregation by industrial methods. In other studies,[33−37] the common features of shish-kebabs were presented: the shish-kebab entity is considerably long, in the range of micrometer, and the diameter of shish is in the range of few nanometers. Moreover, micro-long shish generally align parallel to each other. Additionally, lamellar crystals are approximately a few tens of nanometers thick and their diameter averages at a few tens of nanometers. Moreover, they arrange in periodical stacks with a period of about a few tens of nanometers, exhibiting an ordered nanostructured array. Naturally, such a flow-induced crystallization membrane of shish-kebab aggregation can be considered as a micro/nano hierarchical structure. Accordingly, it remains an issue whether such a micro/nano hierarchical structure of shish-kebab aggregation can be used as the superhydrophobic materials.

Despite the hydrophobicity of nanohybrid shish-kebab paper (i.e., carbon nanotubes act as shish, on which polymer crystal lamellaes are periodically strung along the nanotube axis[38]) can be tuned by polytetrafluoroethylene coatings using initiated chemical vapor deposition.[39] However, to our knowledge, studies on this subject are rare in the open literature, and in particular, there are no studies available on a corresponding pure shish-kebab membrane. The reason is the absence of an efficient way to control pure shish-kebab formation that could form a membrane. This issue has been addressed by our recently developed method via a sheared dilute UHMWPE solution based on a self-made setup.[40] In this study, UHMWPE was crystallized into shish-kebab structure via a flow-induced crystallization method. We first report the wetting behavior of the pure shish-kebab membrane with micro/nano features. The as-prepared membrane is of exceptional superhydrophobicity and excellent self-cleaning effect. Furthermore, the organic contaminants can be easily removed from the water surface, showing the organic liquid uptake ability and recyclability.

EXPERIMENTAL SECTION

Materials. UHMWPE powders were provided by the Second Auxiliary Factory, Beijing, China, with a number-average molecular weight (M_n) in the range of 2.0−3.0 × 10^6 g mol^{-1}. Xylene (analytical reagent, 99%) was purchased from the Tianjin Chemical Reagents Plant. All reagents were used without further purification.

Preparation of Shish-kebab Membrane. UHMWPE powder was first dissolved completely in xylene at 140 °C to obtain a uniform solution with a concentration of 0.058 wt % and then rapidly transferred into a bath pot preset at 105 °C. Flow-induced crystallization was carried out at this temperature using a mechanical stirrer. Ferrum frames were fixed on the stirrer bar so that the frames could rotate synchronously with the stir bar. The schematic of the flow-induced crystallization setup can be found in Figure S1 in the Supporting Information. Continuous stirring was performed at a speed of 800 rpm for 20 min. Then, the pure shish-kebab aggregation in the form of a membrane was dried with hot wind at 60 °C for 3 min, which was defined as a flow-induced crystallization sample (FC, see Figure 1a). For comparison, an uniform UHMWPE solution was cast onto a culture dish and then the sample was cooled down to room temperature at ambient atmosphere. The sample was finally put in an oven to remove the solvent at 80 °C for 7 h, and the upper surface of the sample was defined as a static crystallization sample (SC, see Figure 1a).

Morphology Observation. The morphological characterization was carried out with a scanning electron microscope (SEM, Zeiss MERLIN Compact) at an operating voltage of 5 kV. The samples were sputtered with gold before observation. Additionally, the roughness and morphology of the surfaces were characterized by atomic force microscopy (AFM, Dimension Icon, Bruker) in the tapping mode.

Measurement of Contact Angle and Sliding Angle. The water contact angle was characterized using a drop shape analysis instrument (OCA-20, Data-Physics) at ambient temperature. A water droplet of 9 μL was employed. The sliding angle was measured by tilting the sample stage from 0° to higher angles and then putting a water droplet of 10 μL on the sample using a micro-syringe. Once the droplet can roll off the surface, the angle of the sample stage is considered to be the sliding angle. The detailed processes of water droplet sliding behaviors were recorded by a high-speed video camera (pco.dimax HS1, 7000 fps). The contact angle and sliding angle were the average of five measurements obtained on different positions of the surface.

Droplet Impact Dynamics. The droplet impact dynamic was investigated using a high-speed camera (pco.dimax HS1). Water droplets of 6 μL were used to impact the surfaces at different velocities. The videos were analyzed by the software pco.camware. Of note, all of the measurements regarding droplet dimension and distance were done manually using an open-source image processing software (ImageJ).

DOI: 10.1021/acssuschemeng.8b01047
ACS Sustainable Chem. Eng. 2018, 6, 9866−9875

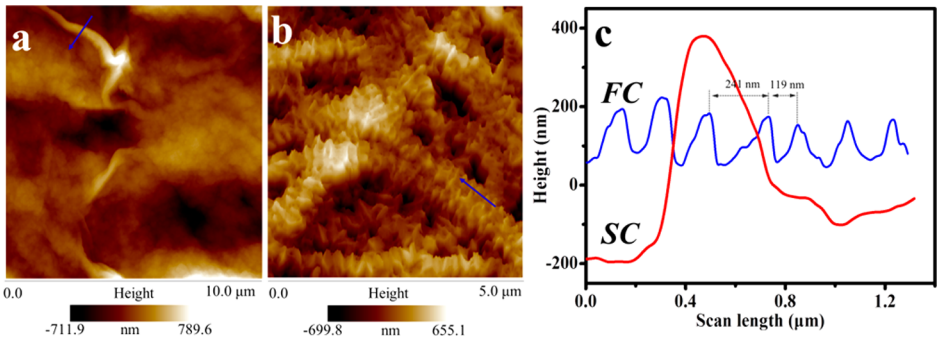

Figure 2. AFM plane images of (a) SC and (b) FC surfaces. (c) Roughness profile of SC and FC surfaces along marked direction.

Self-Cleaning and Antistaining Tests. Manganese dioxide (MnO_2) powder was first deposited on the surface of the as-prepared shish-kebab membrane, and then water droplets were dripped onto the surface with a tilting angle of 20° to test the self-cleaning property. The as-prepared surface was put into $KMnO_4$ dyed water to test the antistaining ability; when the polymer membrane was placed in the culture dish with cyclohexane, the cyclohexane would soak into the polymer membrane immediately due to the lipophilicity of the membrane. The water droplets were dropped onto the as-prepared surface to test an extension of the superhydrophobic effect with non-wettability even when the membrane was soaked in oil.

Membrane Porosity. Membrane porosity (ε) is determined by measuring the dry mass (m_{dry}) and wet mass (m_{wet}) of membrane samples according to eq 1:

$$\varepsilon = \frac{(m_{wet} - m_{dry})/\rho_w}{((m_{wet} - m_{dry})/\rho_w) + (m_{dry}/\rho_m)} \quad (1)$$

where ρ_w and ρ_m are the density of the wetting solvent (ethanol in the current study) and membrane, respectively.

Absorption andRecyclability of the Membrane for OrganicLiquids. Different organic liquids (e.g., soybean oil, diesel oil, cyclohexane, and chloroform) were employed to investigate the absorption capacity of the as-prepared shish-kebab membrane. After the weighted membrane was immersed into organic liquid for 3 min at ambient temperature, the filter paper was used to quickly remove excess oil or organic solvents from the surface to ensure the accuracy of the measurement results. Then its weight was measured again, and the average value reported was derived from at least 5 tested samples. The recyclability of the membrane in the oil absorption test was performed in a centrifuge (TG16-WS). Briefly, in absorption/centrifugation cycles, the soybean oil-absorbed superhydrophobic shish-kebab membrane was regenerated by centrifuge treatment at a rotating speed of 8000 rpm for 10 min, and then the sample was used in further cycles. The weight of the superhydrophobic shish-kebab membrane was recorded before and after each cycle to determine the absorption capacity.

RESULTS AND DISCUSSION

Surface Morphology. The digital photos of the SC and FC membrane are shown in Figure 1a. Macroscopically, both surfaces of the SC and FC membrane are very flat. However, the surface of FC is whiter than that of SC, which should be related to a micro/nano feature and micro-voids in the membrane (see Figure 1b,c). Figure 1b,c presents the SEM images of the SC and FC surfaces. As shown in Figure 1b_1, sparse wrinkles were observed on the SC surface. The high-magnified SEM images reveal the sparse wrinkles with a length of a few microns and a thickness in the range of 150−320 nm (Figure 1b_2,b_3). In contrast, FC is composed of numerous shish-kebabs (Figure 1c_1,c_2). Overall, these shish-kebabs orient along the flow direction (shown by blue arrows in Figure 1c_1). However, they are relatively long (in the scale of micrometer) so that their ends can be hardly distinguished. The amplified images in Figure 1c_2,c_3 demonstrate that many lamellar crystals are decorated perpendicularly to the fibrillar core; such disc-like lamellar crystals are approximately 30 nm thick, and their average diameter is estimated in the range of 128−268 nm. Interestingly, these disc-like lamellar crystals arrange in an ordered nanostructured array. The mechanism of the aforementioned shish-kebabs in a dilute UHMWPE solution under shear flow can be explained using the concept of a coil−stretch transition proposed by Gennes.[41] That is, the UHMWPE chains are generally in an equilibrium with the coiled state in the dilute solution. Once the shear flow is exerted, the long coiled chains could be stretched along the shear direction and then crystallized into shish, on which, the short coiled chains were subsequently adsorbed and crystallized into kebabs.[42] Moreover, many explicit microvoids also exist between the neighboring shish-kebabs as well as those nano-ones between the adjacent kebabs, and the FC membrane is highly porous (porosity: 67−83%), as calculated by eq 1 (Figure 1c_2,b_3). The AFM observation shown in Figure 2a reveals sparse wrinkles on the SC surface. The calculated average roughness (R_a) and root-mean-square roughness (R_q) of the surface by the analysis software of AMF are 158 and 199 nm, respectively. In contrast, for FC, R_a and R_q are, respectively, 166 and 208 nm (Figure 2b). The larger R_a and R_q of FC than that of SC indicate a higher surface roughness of FC. In addition, the height profile along the blue line of Figure 2c shows that the period between the adjacent lamellae in FC is estimated in the range of 119−241 nm. To sum up, the FC surface is the aggregation of shish-kebab with a finely constructed micro/nano hierarchical structure, together with the presence of numerous voids of different scales between the neighboring shish-kebabs as well as the nano-ones between the adjacent kebabs. The stress−strain curves in Figure S2 reveal that the tensile strength of the FC membrane (13.1 MPa) is notably larger than that of the SC membrane (4.6 MPa). The increased tensile strength is ascribed to the structural feature variation from isotropy in the SC membrane to the orientation in the FC membrane,[37,38] which can be confirmed by the 2D-WAXD results in Figure S3.

Wettability and Adhesion Properties of the FC Surface. The results above demonstrate that the FC surface possesses a typical micro/nano hierarchical structure. Many studies have documented that the micro/nano hierarchical structure can lead to the fascinating surface characteristics.[12,43,44,46] Therefore, hydrophobicity of the FC surface is further investigated in the following section. The digital image of water droplets deposited onto the SC and FC surfaces is

DOI: 10.1021/acssuschemeng.8b01047
ACS Sustainable Chem. Eng. 2018, 6, 9866−9875

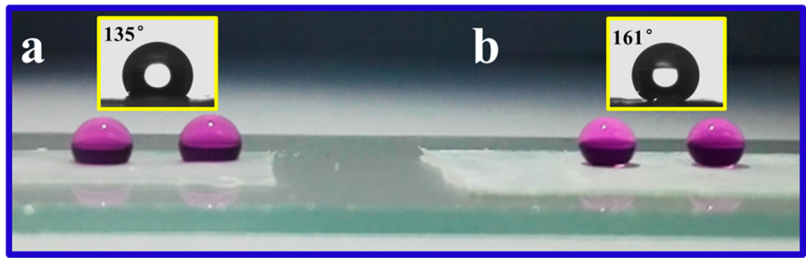

Figure 3. Wettability property of the SC and FC surface. Photograph of water placed on the (a) SC and (b) FC surfaces; inset shows the water contact angle. Water was colored with $KMnO_4$.

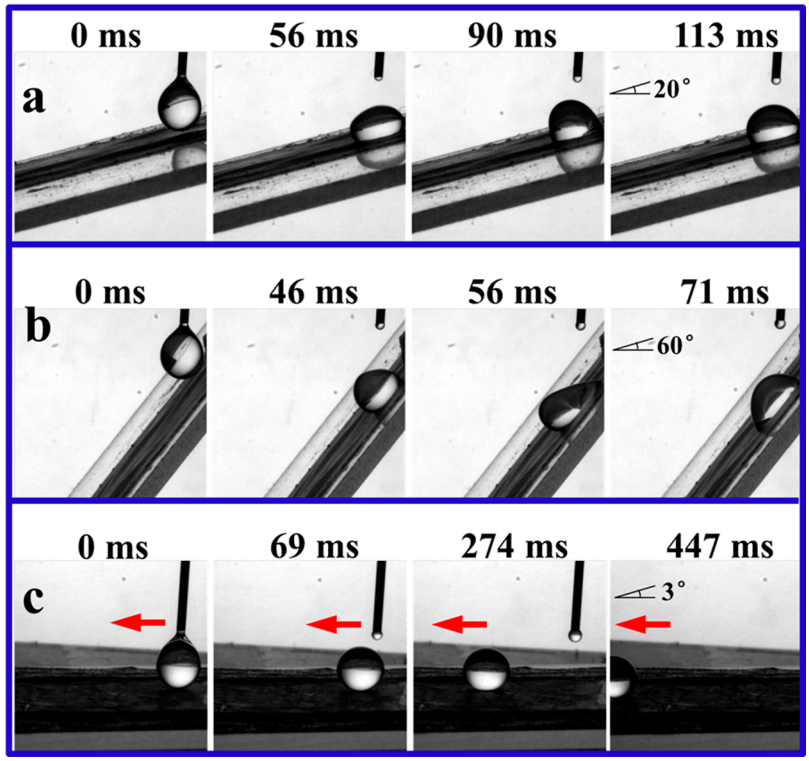

Figure 4. Adhesion property of the SC and FC surface. Process of a 10 μL water droplet dropped on the SC surface, and the water droplet firmly pinned on the surface with a tilting angle of (a) 20° and (b) 60°. (c) Process of a 10 μL water droplet dropped on the FC surface, and the water droplet rolled off the surface within 0.45 s with a tilting angle of 3°.

Table 1. Comparison of Contact Angle and Sliding Angle with Other Literatures' Data

materials	method	contact angle	sliding angle	references
UHWMPE	flow-induced crystallization	161°	3°	our work
PET fabrics	surface-initiated atom transfer radical polymerization	160.5 ± 3°	7 ± 2°	47
PP	polymer reconformation	160°		21
LLDPE	polymer reconformation	153 ± 2°	10°	48
LDPE	lamination templating	160°	5°	49
PANI/cotton fabric	vapor phase deposition	156 ± 2°		50
PP nonwoven fabrics	solvent swelling	159 ± 5°		51
PDMS -coated PU sponge	dip-coating	162 ± 2°		52
PDMS/hydrophobic fumed silica nanoparticle	dip-coating	150 ± 2°		53
PS fibers	electrospinning	151.3 ± 1.6°		54
LDPE	scratching and pricking	154.3 ± 3.2°		55
Poly(alkylpyrrole)	electrochemistry	larger than 150°		56
PI/nanosized silica	electrospinning	157 ± 0.7°	less than 5°	57
PU sponges/polysiloxane	solution immersion	157°		58

presented in Figure 3. As shown in Figure 3a, the droplet exhibits a hemisphere shape on the SC surface, while it almost maintains a spherical shape on the FC surface (Figure 3b). In other words, the contact area between the SC surface and the

DOI: 10.1021/acssuschemeng.8b01047
ACS Sustainable Chem. Eng. 2018, 6, 9866−9875

droplet is larger than that of the FC surface. Quantitatively, the SC surface exhibits a contact angle of 135°, whereas the FC surface shows superhydrophobicity with a contact angle of 161°.

Furthermore, the adhesive property of the SC and FC surfaces was investigated. Figure 4a,b shows the process of a 10 μL water droplet dripping on the SC surface with different tilting angles. As for SC with a tilting angle of 20°, the water droplet tightly pins on the surface and cannot roll away (Figure 4a and Movie S1 in Supporting Information). Even the tilting angle turned to 60°, the water droplet still firmly stuck on the SC surface (Figure 4b and Movie S2 in Supporting Information). Such a case demonstrates a highly strong water adhesion between the water droplet and the SC surface. It is very interesting to note that, once a 10 μL water droplet contacts the surface of FC with a tilting angle of 3° (see Figure 4c), it begins to slide immediately, and the water droplet slides across the field of view rapidly within 0.45 s (Movie S3 in Supporting Information). This rolling process clearly demonstrates that the FC surface has an excellent water-repellent property with a sliding angle as low as 3°. To sum up, the SC surface is of hydrophobicity with strong water adhesion, whereas the FC surface is of superhydrophobicity with a low water adhesion. For comparison, Table 1 shows the contact angle and sliding angle of this study as well as those in other studies concerning the polymer hydrophobic surfaces, demonstrating excellent superhydrophobicity of FC surface in this study. As mentioned above, the FC surface is of micro/nano hierarchical structure, together with the presence of numerous voids with different sizes. Such micro/nano hierarchical structure leads to a composite interface in which air becomes trapped within the grooves, leading to the hydrophobicity transition of UHWMPE from the hydrophobic surface to the superhydrophobic surface. To further understand the superhydrophobicity of FC, the apparent water contact angle is described by the Cassie equation:[45]

$$\cos\theta^* = -1 + f(\cos\theta + 1) \quad (2)$$

where, f is the solid fraction that the liquid is in contact with, and θ^* (161°) and θ (106°) are, respectively, the water contact angles on the FC surface and the smooth UHMWPE surface (detailed information can be found in Figures S4 and S5 in the Supporting Information). According to the above equation, it is easily calculated that the solid fraction that the liquid is in contact with is equal to about 0.07. In other words, large-area air (93%) can immerse into the interspaces of the FC surface. This result further demonstrates that the superhydrophobic and slippery property of FC should be ascribed to the micro/nano hierarchical structure with abundant air fraction.

Droplet Impact on the FC Surface. In practical applications, the impingement of water droplets on surfaces with different wettability is always encountered.[59] For the purpose of a comparison between these two surfaces, a water-droplet impact experiment was performed, and water droplets of 6 μL were used to impact the surfaces at a velocity of 1.08 m/s (fall height of 6 cm). The impingement process of water droplets on the surface was captured using a high-speed camera (7000 fps). Figure 5a shows the sequential images of a water droplet impinging on the SC surface. Obviously, once the water droplet impacts the SC surface, it reaches the maximum spread and exhibits a complete wetting state after the impingement. Moreover, no evidence of the bouncing effect can be found (Movie S4 in Supporting Information). In

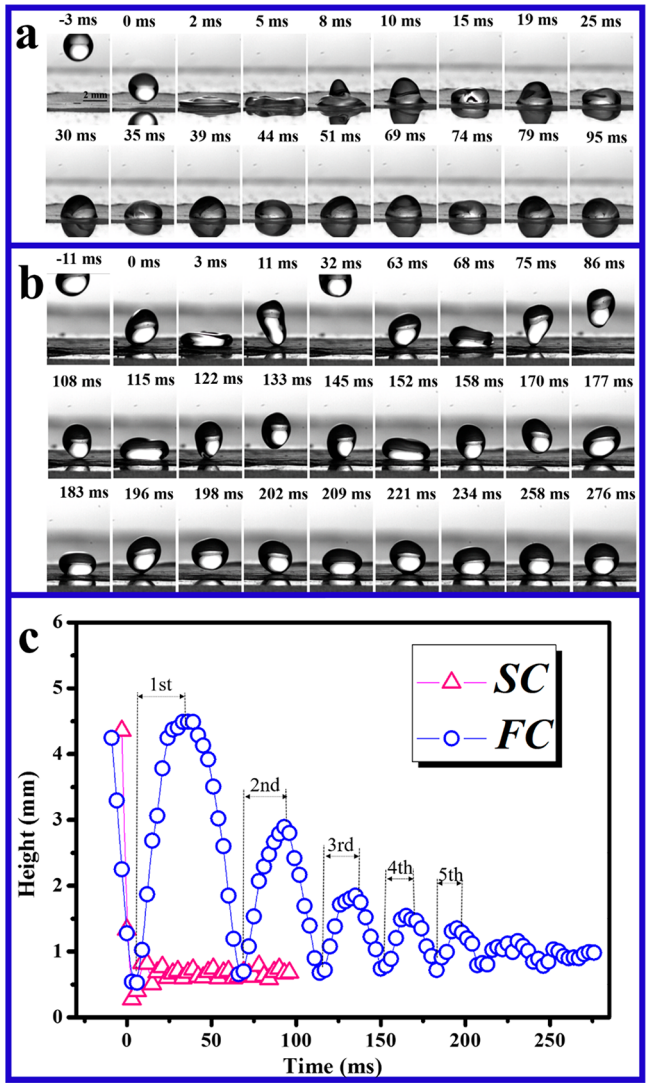

Figure 5. Droplet impact on the SC and FC surfaces. Time evolution of droplet-impact dynamics upon the (a) SC and (b) FC surfaces. (c) Water droplets rebound height as a function of time.

other words, the SC surface tends to capture the impacted droplet and drains it along the substrate. Such phenomena should be attributed to the relatively large vertical adhesive force between the water droplet and the SC surface. In contrast, once the droplet first impacts the FC surface, it changes into a "pancake" shape at 3 ms and bounces off the surface at approximately 11 ms with an emission of a water jet (see Figure 5b and Movie S5 in the Supporting Information). After the first bounce from the surface, the kinetic energy of the water droplet is gradually attenuated, and the maximum height of the bouncing drop is therefore lower than the last bounce. More importantly, any evidence of water droplet residue is hardly observed on the FC surface during the whole impingement process. This phenomenon suggests that the FC surface has an excellent antiwetting performance during the dynamic droplet impact. Figure 5c quantitatively shows the rebound height of the water droplet on the SC and FC surfaces as a function of time. The significant difference between these two surfaces can be clearly observed: the water droplet can bounce off the FC surface five times, showing an extended bouncing process for longer periods of time (202 ms).

DOI: 10.1021/acssuschemeng.8b01047
ACS Sustainable Chem. Eng. 2018, 6, 9866−9875

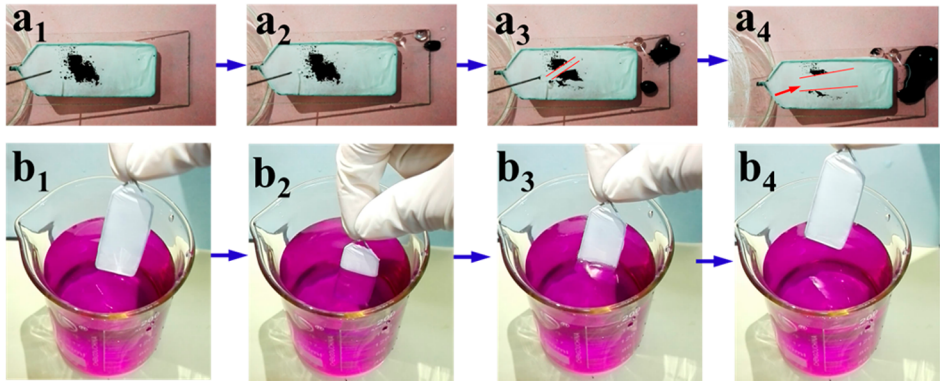

Figure 6. Self-cleaning and antistaining properties of the FC surface. (a) Self-cleaning process of the FC surface with MnO_2 powder as a model of contaminant. Contaminated surface with water droplets on them (a_2) and (a_3) as well as after water droplets slide across the surface (a_4). (b) FC was inserted into $KMnO_4$ dyed water, showing that the membrane was not dyed due to its anti-staining property.

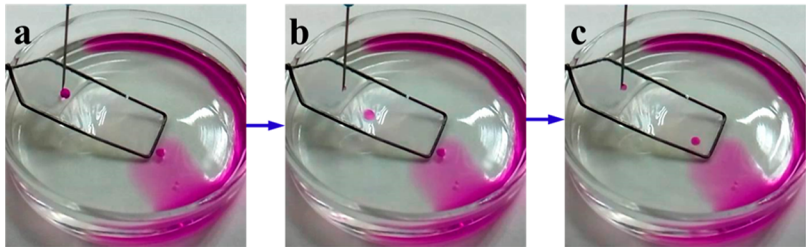

Figure 7. Water was dropped onto the FC surface to test the superhydrophobic ability after the surface was contaminated by oil.

Whereas, the water droplet stays pinning to the SC surface, showing no bouncing effect because of the drastic depletion of kinetic energy.

As is well-known, an effective water hammer pressure (P_{WH}) can be generated at the contact stage when the superhydrophobic surface suffers from a water droplet impact.[60] The P_{WH} can be approximated as[61]

$$P_{WH} \approx 0.2\rho CV \tag{3}$$

where ρ is the water density, C is the sound velocity in water ($C \sim 1497$ m/s and $\rho \sim 1000$ kg/m^3), and V is the velocity of the water droplet. The change of the wetting state of the rough surface depends on the balance between P_{WH} and the capillary pressure ($P_{capillary}$) generated within the surface texture.[61,62] In this study, water droplets of 6 μL were used to impact the surfaces at different velocities to estimate P_{WH} and $P_{capillary}$. The impingement process of water droplets on the surface was captured using a high-speed camera (7000 fps). In the case of water droplet with an impinging speed of 2.470 m/s (fall height of 31 cm), the calculated P_{WH} is 0.740 MPa, according to eq 2. As can be seen in Figure S6a, after the water droplet impacts the FC surface, it changes into a "pancake" shape surrounded with some satellite droplets at 3 ms. These satellite droplets can bounce off the FC surface to assemble into a large water droplet (see Figure S6a at 8 and 13 ms). Such a large water droplet can completely lift off the surface (see Figure S6a at 22 ms). After the large water droplet bounces from the surface, it stays on the FC surface (see Figure S6a at 32 and 50 ms as well as Movie S6 in the Supporting Information). In view of this, the calculated P_{WH} (0.740 MPa) might be smaller than the $P_{capillary}$ generated from the shish-kebab surface, and therefore the droplet presents a nonwetting state. In contrast, when the water droplet is used to impact the surface at a velocity of 2.617 m/s (fall height of 35 cm), it reaches the maximum spread surrounded with some satellite droplets (see Figure S6b at 5 ms), and these satellite droplets cannot bounce but pin to the FC surface to form a large water droplet (see Figure S6b at 12 and 16 ms). Moreover, the large water droplet is tightly captured by the FC surface (see Figure S6b at 18 and 27 ms). In other words, such a large droplet can penetrate into the surface during the impingement stage, exhibiting a total wetting state after the impingement (see Figure S6b at 39 ms and Movie S7 in the Supporting Information). In this case, according to eq 3, the calculated P_{WH} is 0.784 MPa, and therefore $P_{capillary}$ is smaller than P_{WH} (0.784 MPa). The pressure discussed here will help to control the wetting behavior of the FC surface to achieve a nonwetting state when the P_{WH} is smaller than the $P_{capillary}$ (~0.740 MPa).

Self-Cleaning and Antistaining Properties of the FC Surface. The interesting superhydrophobicity and low water adhesion of the surface with shish-kebab aggregation motivated us to investigate the self-cleaning ability. As shown in Figure 6a_1–a_3, when the water droplets are dripped onto the contaminated surface, the powders on the FC surface are immediately swept off by the water droplets (Movie S8 in the Supporting Information). As a result, no contaminant is visible on the FC surface where the water droplets slide across (shown by red arrow in Figure 6a_4). This should be ascribed to the joint action of high capillary forces induced by water droplets and weak adhesion of the contaminant powders to the superhydrophobic surface.[63] The antistaining property test experiment was designed. The result is shown in Figure 6b and Movie S9 in the Supporting Information. The FC membrane is first dipped into the $KMnO_4$ dyed water for 10 s (Figure 6b_1,b_2). After FC is taken out from the solution, no traces of contamination can be found on the surface (Figure 6b_3,b_4), suggesting that the FC surface possesses excellent antistaining property. Moreover, the non-wettability test of the FC surface

DOI: 10.1021/acssuschemeng.8b01047
ACS Sustainable Chem. Eng. 2018, 6, 9866–9875

after oil (cyclohexane) contamination was also carried out (Figure 7a–c). Obviously, although the FC surface is contaminated by cyclohexane, water droplets can still slide easily without wetting the FC surface, indicating that the FC surface maintains its superhydrophobic property even being contaminated by oil (Movie S10 in the Supporting Information). In a word, the above results suggest that the FC possesses excellent self-cleaning and anti-staining properties, and such a superhydrophobic surface can protect substrates from pollution in practical applications.[63]

Oil/Water Separation by the FC Membrane. The above results demonstrate that the FC surface not only contains numerous voids and high porosity in micro/nano scale but also shows superhydrophobicity. In addition, the voids in the different scales between the neighboring shish-kebabs as well as the nano-ones between the adjacent kebabs provide storage space. It is well-known that polyethylene is intrinsically hydrophobic-lipophilic.[64] Therefore, we speculate that the voids and superhydrophobicity should give a good oil/water separation capacity. In this oil/water separation experiment, cyclohexane dyed with Sudan Red is first dripped onto the middle of the water surface to form a thin layer (Figure 8a).

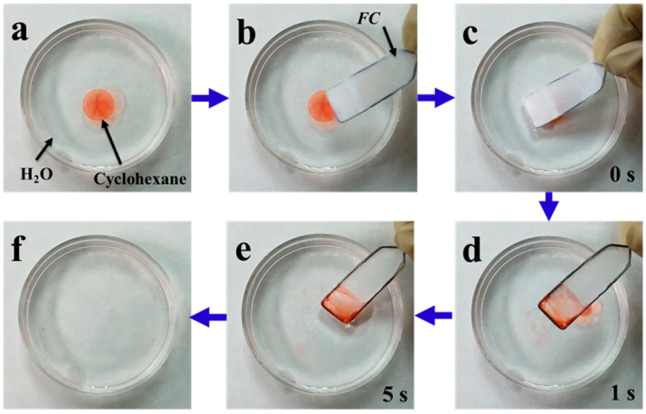

Figure 8. Oil/water separation by the FC membrane. (a–f) Images of the removal processes of cyclohexane from water using the FC membrane.

Once the FC membrane touches the cyclohexane layer on the water surface, cyclohexane is fully absorbed within a few seconds (Figure 8b–e). Finally, the contaminated water is cleaned, and no trace of cyclohexane can be found (Figure 8f). This result implies that FC is oleophilic and shows oil/water separation ability. Movie S11 in the Supporting Information shows how quickly FC can absorb the cyclohexane layer. The excellent oil/water separation capability of the FC membrane is mainly ascribed to two aspects. On one hand, polyethylene is intrinsically hydrophobic-lipophilic, and the as-prepared FC exhibits superhydrophobicity because the FC surface possesses a hierarchical micro/nano feature. On the other hand, oil can be driven through the voids of the membrane into its bulk in the presence of a capillary force, while water is completely excluded by the superhydrophobic surface, resulting in separating oil from water.[65]

To further investigate the organic liquids (e.g., soybean oil, diesel oil, cyclohexane, and chloroform) absorption capacity of the as-prepared membranes, the adsorption test was performed. The absorption capacity (k) was calculated by the weight-gain ratio according to eq 4:

$$k = (M_2 - M_1)/M_1 \quad (4)$$

where M_1 and M_2, respectively, represent the weight of the as-prepared membrane before and after absorption of oil or organic solvent. As shown in Figure 9a, FC not only absorbs organic liquids but also exhibits a higher absorption capacity ranging from 15 to 32 times of its own weight, depending on the viscosity and density of the organic liquids. However, SC can absorb organic liquids at 4 to 7 times its own weight. To sum up, the absorption capacity of FC is remarkably higher than that of SC. Figure 9b shows the recyclability of the membrane in soybean oil absorption. The membrane basically retained its high absorbency after 10 cycles. The higher absorption capacity and recyclability of FC for different organic liquids will guarantee its promising application for oil/water separation purposes.

CONCLUSIONS

In summary, we first report the wetting behavior of the pure shish-kebab membrane. The membrane exhibits a micro/nano hierarchical structure, displaying a superhydrophobic characteristic with a static water contact angle of 161° and sliding angle of 3°. Moreover, the membrane with low adhesion is resistant to droplet impact, showing an extended bouncing process for longer periods of time (202 ms). The water hammer pressure discussed here will help to control the wetting behavior of the FC surface to completely achieve a nonwetting state. Importantly, such a membrane not only

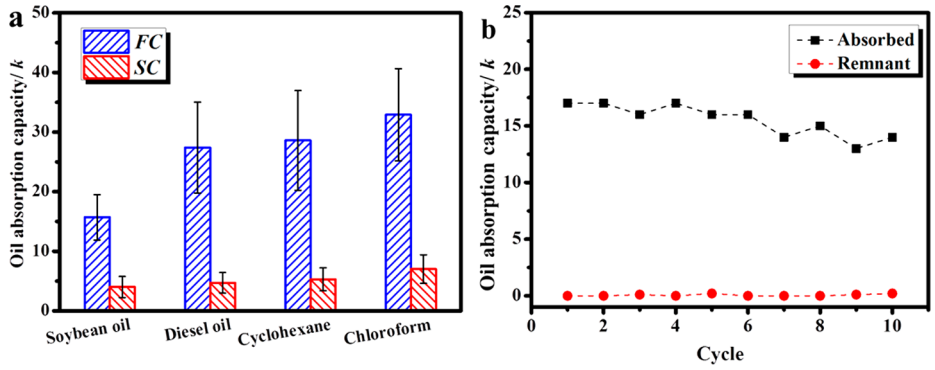

Figure 9. (a) Absorption capacities of the FC and SC membrane toward organic liquids. (b) Oil-absorption capacity of the FC membrane with different absorption/centrifugation cycles. The "Remnant" represent the weight of the FC membrane in each cycle after centrifugation, and the "Absorbed" represent the weight of FC membrane in each cycle before centrifugation.

DOI: 10.1021/acssuschemeng.8b01047
ACS Sustainable Chem. Eng. 2018, 6, 9866–9875

shows excellent self-cleaning and antistaining properties but also shows oil/water separation capacity, high absorption capacity ranging from 15 to 32 times of its own weight, and recyclability for organic liquids. This study clearly indicates that micro/nano hierarchical structure of pure shish-kebab aggregation can be used as the superhydrophobic materials. Moreover, this study well demonstrates that intricate instruments, tedious and time-consuming treatments, or processing and specialized nanomaterials are not necessary to prepare a superhydrophobic surface.

■ ASSOCIATED CONTENT

Supporting Information

The Supporting Information is available free of charge on the ACS Publications website at DOI: 10.1021/acssuschemeng.8b01047.

The preparation procedure of smooth UHWMPE surface, method of mechanical property test, structural characterization of the membranes, schematic of a modified flow-induced crystallization setup used in this study, representative stress−strain curves of the SC membrane and FC membrane, 2D-WAXD patterns for SC and FC, SEM image of smooth UHWMPE surface, AFM plane image of smooth UHWMPE surface, roughness profile of smooth UHWMPE surface, and sequential photographs of 6 μL of water droplet impinging on the FC surface at different velocities (PDF)

High-speed video of a 10 μL water droplet dropping on the SC surface with a tilting angle of 20° (AVI)

High-speed video of a 10 μL water droplet dropping on the SC surface with a tilting angle of 60° (AVI)

High-speed video of a 10 μL water droplet dropping on the FC surface with a tilting angle of 3° (AVI)

High-speed video of a 6 μL water droplet impinging the SC surface with an impacting velocity of 1.4 m/s (AVI)

High-speed video of a 6 μL water droplet impinging the FC surface with an impacting velocity of 1.4 m/s (AVI)

High-speed video of a 6 μL water droplet impinging the FC surface with an impacting velocity of 2.470 m/s (AVI)

High-speed video of a 6 μL water droplet impinging the FC surface with an impacting velocity of 2.617 m/s (AVI)

Self-cleaning test on the FC membrane; water droplets are used to remove dirt (MnO_2 powder) from the FC surface (AVI)

Self-cleaning and anti-wetting test on the FC membrane; the FC membrane is inserted into $KMnO_4$ dyed water and then taken out (AVI)

Self-cleaning test of the FC surface after oil (hexadecane) contamination; water droplets slide off from the surface which is immersed in oil (AVI)

Oil-water separation test on the FC membrane; when the FC membrane touches the cyclohexane layer on the water surface, it completely realizes oil-water separation within a few seconds (AVI)

■ AUTHOR INFORMATION

Corresponding Authors

*E-mail: xianhu.liu@zzu.edu.cn.

*E-mail: gqzheng@zzu.edu.cn.

*E-mail: zguo10@utk.edu.

ORCID

Kun Dai: 0000-0002-9877-8552

Zhanhu Guo: 0000-0003-0134-0210

Notes

The authors declare no competing financial interest.

■ ACKNOWLEDGMENTS

The authors are grateful for the financial support from the National Natural Science Foundation of China (11432003, 11572290), the Major State Basic Research Projects (2012CB025904), HASTIT, and the Plan for Scientific Innovation Talent of Henan Province. Z.G. appreciates the start-up funds from University of Tennessee.

■ REFERENCES

(1) Li, Y.; Dai, S.; John, J.; Carter, K. R. Superhydrophobic surfaces from hierarchically structured wrinkled polymers. *ACS Appl. Mater. Interfaces* **2013**, *5*, 11066−11073.

(2) Jiang, L.; Yao, X.; Li, H.; Fu, Y.; Chen, L.; Meng, Q.; Hu, W.; Jiang, L. "Water strider" legs with a self-assembled coating of single-crystalline nanowires of an organic semiconductor. *Adv. Mater.* **2010**, *22*, 376−379.

(3) Xu, L.; Tong, F.; Lu, X.; Lu, K.; Lu, Q. Multifunctional polypyrene/silica hybrid coatings with stable excimer fluorescence and robust superhydrophobicity derived from electrodeposited polypyrene films. *J. Mater. Chem. C* **2015**, *3*, 2086−2092.

(4) Wang, S.; Jiang, L. Definition of Superhydrophobic States. *Adv. Mater.* **2007**, *19*, 3423−3424.

(5) Nakajima, A.; Fujishima, A.; Hashimoto, K.; Watanabe, T. Preparation of transparent superhydrophobic boehmite and silica films by sublimation of aluminum acetylacetonate. *Adv. Mater.* **1999**, *11*, 1365−1368.

(6) Gao, S.; Sun, J.; Liu, P.; Zhang, F.; Zhang, W.; Yuan, S.; Li, J.; Jin, J. A robust polyionized hydrogel with an unprecedented underwater anti-crude-oil-adhesion property. *Adv. Mater.* **2016**, *28*, 5307−5314.

(7) Ge, J.; Zhang, J.; Wang, F.; Li, Z.; Yu, J.; Ding, B. Superhydrophilic and underwater superoleophobic nanofibrous membrane with hierarchical structured skin for effective oil-in-water emulsion separation. *J. Mater. Chem. A* **2017**, *5*, 497−502.

(8) (a) Wang, Y.; Liu, X.; Lian, M.; Zheng, G.; Dai, K.; Guo, Z.; Liu, C.; Shen, C. Continuous fabrication of polymer microfiber bundles with interconnected microchannels for oil/water separation. *Appl. Mater. Today* **2017**, *9*, 77−81. (b) Zhang, M.; Dong, M.; Chen, S.; Guo, Z. Slippery liquid-infused porous surface fabricated on aluminum maintain stable corrosion resistance at elevated temperatures. *Eng. Sci.* **2018**, DOI: 10.30919/es8d732.

(9) Miwa, M.; Nakajima, A.; Fujishima, A.; Hashimoto, K.; Watanabe, T. Effects of the surface roughness on sliding angles of water droplets on superhydrophobic surfaces. *Langmuir* **2000**, *16*, 5754−5760.

(10) Nakajima, A.; Watanabe, T.; Takai, K.; Yamauchi, G.; Fujishima, A.; Hashimoto, K. Transparent superhydrophobic thin films with self-cleaning properties. *Langmuir* **2000**, *16*, 7044−7047.

(11) Shibuichi, S.; Yamamoto, T.; Onda, T.; Tsujii, K. Super water- and oil-repellent surfaces resulting from fractal structure. *J. Colloid Interface Sci.* **1998**, *208*, 287−294.

(12) Genzer, J.; Efimenko, K. Creating long-lived superhydrophobic polymer surfaces through mechanically assembled monolayers. *Science* **2000**, *290*, 2130−2133.

(13) Schondelmaier, D.; Cramm, S.; Klingeler, R.; Morenzin, J.; Zilkens, C.; Eberhardt, W. Orientation and self-assembly of hydrophobic fluoroalkylsilanes. *Langmuir* **2002**, *18*, 6242−6245.

(14) Qi, Y.; Cui, Z.; Liang, B.; Parnas, R. S.; Lu, H. A fast method to fabricate superhydrophobic surfaces on zinc substrate with ion assisted chemical etching. *Appl. Surf. Sci.* **2014**, *305*, 716−724.

(15) Qian, B.; Shen, Z. Fabrication of superhydrophobic surfaces by dislocation-selective chemical etching on aluminum, copper, and zinc substrates. *Langmuir* **2005**, *21*, 9007−9009.
(16) Xue, C.; Guo, X.; Ma, J.; Jia, S. Fabrication of robust and antifouling superhydrophobic surfaces via surface-initiated atom transfer radical polymerization. *ACS Appl. Mater. Interfaces* **2015**, *7*, 8251−8259.
(17) Li, X.; Shen, J. A facile two-step dipping process based on two silica systems for a superhydrophobic surface. *Chem. Commun.* **2011**, *47*, 10761−10763.
(18) Zhang, G.; Wang, D.; Gu, Z. Z.; Möhwald, H. Fabrication of superhydrophobic surfaces from binary colloidal assembly. *Langmuir* **2005**, *21*, 9143−9148.
(19) Kang, H.; Cheng, Z.; Lai, H.; Ma, H.; Liu, Y.; Mai, X.; Wang, Y.; Shao, Q.; Xiang, L.; Guo, X.; Guo, Z. Superlyophobic anti-corrosive and self-cleaning titania robust mesh membrane with enhanced oil/water separation. *Sep. Purif. Technol.* **2018**, *201*, 193−204.
(20) Li, Y.; Liu, F.; Sun, J. A facile layer-by-layer deposition process for the fabrication of highly transparent superhydrophobic coatings. *Chem. Commun.* **2009**, *19*, 2730−2732.
(21) Erbil, H. Y.; Demirel, A. L.; Avci, Y.; Mert, O. Transformation of a simple plastic into a superhydrophobic surface. *Science* **2003**, *299* (5611), 1377−1380.
(22) Lu, X.; Zhang, C.; Han, Y. Low-Density Polyethylene Superhydrophobic Surface by Control of Its Crystallization Behavior. *Macromol. Rapid Commun.* **2004**, *25*, 1606−1610.
(23) Ma, M.; Mao, Y.; Gupta, M.; Gleason, K. K.; Rutledge, G. C. Superhydrophobic fabrics produced by electrospinning and chemical vapor deposition. *Macromolecules* **2005**, *38*, 9742−9748.
(24) Liu, Z.; Wang, H.; Wang, E.; Zhang, X.; Yuan, R.; Zhu, Y. Superhydrophobic poly(vinylidene fluoride) membranes with controllable structure and tunable wettability prepared by one-step electrospinning. *Polymer* **2016**, *82*, 105−113.
(25) Xu, Q. F.; Mondal, B.; Lyons, A. M. Fabricating superhydrophobic polymer surfaces with excellent abrasion resistance by a simple lamination templating method. *ACS Appl. Mater. Interfaces* **2011**, *3*, 3508−3514.
(26) Jiang, L.; Wang, R.; Yang, B.; Li, T. J.; Tryk, D. A.; Fujishima, A.; Hashimoto, K.; Zhu, D. B. Binary cooperative complementary nanoscale interfacial materials. *Pure Appl. Chem.* **2000**, *72*, 73−81.
(27) Huang, Y.; Gao, A.; Song, X.; Shu, D.; Yi, F.; Zhong, J.; Zeng, R.; Zhao, S.; Meng, T. Supramolecule-inspired fabrication of carbon nanoparticles in-situ anchored graphene nanosheets material for high-performance supercapacitors. *ACS Appl. Mater. Interfaces* **2016**, *8*, 26775−26782.
(28) Tian, Y.; Zhu, C.; Gong, J.; Ma, J.; Xu, J. Transition from shish-kebab to fibrillar crystals during ultra-high hot stretching of ultra-high molecular weight polyethylene fibers: in situ small and wide angle X-ray scattering studies. *Eur. Polym. J.* **2015**, *73*, 127−136.
(29) Sobieraj, M. C.; Rimnac, C. M. Ultra high molecular weight polyethylene: mechanics, morphology, and clinical behavior. *J. Biomed. Mater.* **2009**, *2*, 433−443.
(30) Ronca, S.; Forte, G.; Ailianou, A.; Kornfield, J. A.; Rastogi, S. Direct route to colloidal UHMWPE by including LLDPE in solution during homogeneous polymerization of ethylene. *ACS Macro Lett.* **2012**, *1*, 1116−1120.
(31) Keller, A.; Kolnaar, H. W. H. Flow-induced orientation and structure formation. *Mater. Sci. Tech-Lond* **1997**, *18*, 190.
(32) Liu, X.; Dai, K.; Hao, X.; Zheng, G.; Liu, C.; Schubert, D. W.; Shen, C. Crystalline structure of injection molded β-isotactic polypropylene: Analysis of the oriented shear zone. *Ind. Eng. Chem. Res.* **2013**, *52*, 11996−12002.
(33) Hsiao, B. S.; Yang, L.; Somani, R. H.; Avila-Orta, C. A.; Zhu, L. Unexpected shish-kebab structure in a sheared polyethylene melt. *Phys. Rev. Lett.* **2005**, *94*, 117802.
(34) Kimata, S.; Kornfield, J. A.; Sakurai, T.; Nozue, Y.; Kasahara, T.; Yamaguchi, N.; Karino, T.; Shibayama, M. Molecular basis of the shish-kebab morphology in polymer crystallization. *Science* **2007**, *316*, 1014−1017.
(35) Geng, L.; Li, L.; Mi, H.; Chen, B.; Sharma, P.; Ma, H.; Hsiao, B. S.; Peng, X.; Kuang, T. Superior Impact Toughness and Excellent Storage Modulus of Poly (lactic acid) Foams Reinforced by Shish-Kebab Nanoporous Structure. *ACS Appl. Mater. Interfaces* **2017**, *9*, 21071−21076.
(36) Peng, X.; Chen, J.; Kuang, T.; Yu, P.; Huang, J. Simultaneous reinforcing and toughening of high impact polystyrene with a novel processing method of loop oscillating push−pull molding. *Mater. Lett.* **2014**, *123*, 55−58.
(37) Qin, Y.; Xu, Y.; Zhang, L.; Zheng, G.; Dai, K.; Liu, C.; Guo, Z.; Yan, X.; Guo, Z. Shear-induced interfacial sheath structure in isotactic polypropylene/glass fiber composites. *Polymer* **2015**, *70*, 326−335.
(38) Liang, S.; Wang, K.; Chen, D.; Zhang, Q.; Du, R.; Fu, Q. Shear enhanced interfacial interaction between carbon nanotubes and polyethylene and formation of nanohybrid shish-kebabs. *Polymer* **2008**, *49*, 4925−4929.
(39) Laird, E. D.; Bose, R. K.; Qi, H.; Lau, K. K.; Li, C. Electric field-induced, reversible lotus-to-rose transition in nanohybrid shish kebab paper with hierarchical roughness. *ACS Appl. Mater. Interfaces* **2013**, *5*, 12089−12098.
(40) Zheng, H.; Quan, Y.; Zheng, G.; Dai, K.; Liu, C.; Shen, C. Fabrication of a polymer/aligned shish-kebab composite: microstructure and mechanical properties. *RSC Adv.* **2015**, *5*, 60392−60400.
(41) De Gennes, P. G. Coil-stretch transition of dilute flexible polymers under ultrahigh velocity gradients. *J. Chem. Phys.* **1974**, *60*, 5030−5042.
(42) Dukovski, I.; Muthukumar, M. Langevin dynamics simulations of early stage shish-kebab crystallization of polymers in extensional flow. *J. Chem. Phys.* **2003**, *118*, 6648−6655.
(43) Onda, T.; Shibuichi, S.; Satoh, N.; Tsujii, K. Super-Water-Repellent Fractal Surfaces. *Langmuir* **1996**, *12*, 2125−2127.
(44) Tadanaga, K.; Katata, N.; Minami, T. Formation process of super-water-repellent Al_2O_3 coating films with high transparency by the sol-gel method. *J. Am. Ceram. Soc.* **1997**, *80*, 3213−3216.
(45) Drelich, J.; Wilbur, J. L.; Miller, J. D.; Whitesides, G. M. Contact angles for liquid drops at a model heterogeneous surface consisting of alternating and parallel hydrophobic/hydrophilic strips. *Langmuir* **1996**, *12*, 1913−1922.
(46) Feng, L.; Li, S.; Li, H.; Zhai, J.; Song, Y.; Jiang, L.; Zhu, D. Super-hydrophobic surface of aligned polyacrylonitrile nanofibers. *Angew. Chem.* **2002**, *114*, 1269−1271.
(47) Xue, C.; Guo, X.; Ma, J.; Jia, S. Fabrication of robust and antifouling superhydrophobic surfaces via surface-initiated atom transfer radical polymerization. *ACS Appl. Mater. Interfaces* **2015**, *7*, 8251−8259.
(48) Yuan, Z.; Chen, H.; Zhang, J.; Zhao, D.; Liu, Y.; Zhou, X.; Chen, X.; Li, S.; Shi, P.; Tang, J. Preparation and characterization of self-cleaning stable superhydrophobic linear low-density polyethylene. *Sci. Technol. Adv. Mater.* **2008**, *9*, 045007.
(49) Xu, Q.; Mondal, B.; Lyons, A. M. Fabricating superhydrophobic polymer surfaces with excellent abrasion resistance by a simple lamination templating method. *ACS Appl. Mater. Interfaces* **2011**, *3*, 3508−3514.
(50) Zhou, X.; Zhang, Z.; Xu, X.; Guo, F.; Zhu, X.; Men, X.; Ge, B. Robust and durable superhydrophobic cotton fabrics for oil/water separation. *ACS Appl. Mater. Interfaces* **2013**, *5*, 7208−7214.
(51) Zhu, T.; Cai, C.; Duan, C.; Zhai, S.; Liang, S.; Jin, Y.; Zhao, N.; Xu, J. Robust polypropylene fabrics super-repelling various liquids: a simple, rapid and scalable fabrication method by solvent swelling. *ACS Appl. Mater. Interfaces* **2015**, *7*, 13996−14003.
(52) Wang, C.; Lin, S. Robust superhydrophobic/superoleophilic sponge for effective continuous absorption and expulsion of oil pollutants from water. *ACS Appl. Mater. Interfaces* **2013**, *5*, 8861−8864.
(53) Cao, M.; Guo, D.; Yu, C.; Li, K.; Liu, M.; Jiang, L. Water-repellent properties of superhydrophobic and lubricant-infused

DOI: 10.1021/acssuschemeng.8b01047
ACS Sustainable Chem. Eng. 2018, 6, 9866−9875

"slippery" surfaces: a brief study on the functions and applications. *ACS Appl. Mater. Interfaces* **2016**, *8*, 3615−3623.
(54) Wu, J.; Wang, N.; Wang, L.; Dong, H.; Zhao, Y.; Jiang, L. Electrospun porous structure fibrous film with high oil adsorption capacity. *ACS Appl. Mater. Interfaces* **2012**, *4*, 3207−3212.
(55) Zhao, T.; Zhang, D.; Yu, C.; Jiang, L. Facile fabrication of a polyethylene mesh for oil/water separation in complex environment. *ACS Appl. Mater. Interfaces* **2016**, *8*, 24186−24191.
(56) Yan, H.; Kurogi, K.; Mayama, H.; Tsujii, K. Environmentally stable super water-repellent poly(alkylpyrrole) films. *Angew. Chem., Int. Ed.* **2005**, *44*, 3453−3456.
(57) Gong, G.; Gao, K.; Wu, J.; Sun, N.; Zhou, C.; Zhao, Y.; Jiang, L. A highly durable silica/polyimide superhydrophobic nanocomposite film with excellent thermal stability and abrasion-resistant performance. *J. Mater. Chem. A* **2015**, *3*, 713−718.
(58) Zhu, Q.; Chu, Y.; Wang, Z.; Chen, N.; Lin, L.; Liu, F.; Pan, Q. Robust superhydrophobic polyurethane sponge as a highly reusable oil-absorption material. *J. Mater. Chem. A* **2013**, *1*, 5386−5393.
(59) Chen, L.; Xiao, Z.; Chan, P.; Lee, Y. K.; Li, Z. A comparative study of droplet impact dynamics on a dual-scaled superhydrophobic surface and lotus leaf. *Appl. Surf. Sci.* **2011**, *257*, 8857−8863.
(60) Xu, L.; Tong, F.; Lu, X.; Lu, K.; Lu, Q. Multifunctional polypyrene/silica hybrid coatings with stable excimer fluorescence and robust superhydrophobicity derived from electrodeposited polypyrene films. *J. Mater. Chem. C* **2015**, *3*, 2086−2092.
(61) Deng, T.; Varanasi, K. K.; Hsu, M.; Bhate, N.; Keimel, C.; Stein, J.; Blohm, M. Nonwetting of impinging droplets on textured surfaces. *Appl. Phys. Lett.* **2009**, *94*, 133109.
(62) Checco, A.; Rahman, A.; Black, C. T. Robust superhydrophobicity in large-area nanostructured surfaces defined by block-copolymer self assembly. *Adv. Mater.* **2014**, *26*, 886−891.
(63) Su, F.; Yao, K. Facile fabrication of superhydrophobic surface with excellent mechanical abrasion and corrosion resistance on copper substrate by a novel method. *ACS Appl. Mater. Interfaces* **2014**, *6*, 8762−8770.
(64) Herkenberg, W. Method for the removal of oil from oil spills. U.S. Patent US5451325, 1995.
(65) Bi, H.; Xie, X.; Yin, K.; Zhou, Y.; Wan, S.; He, L.; Ruoff, R. S.; Xu, F.; Banhart, F.; Sun, L. Spongy graphene as a highly efficient and recyclable sorbent for oils and organic solvents. *Adv. Funct. Mater.* **2012**, *22*, 4421−4425.

DOI: 10.1021/acssuschemeng.8b01047
ACS Sustainable Chem. Eng. 2018, 6, 9866−9875